INTEGRATED VIDEO-SEDIMENT TRACER TECHNIQUE FOR SAND TRANSPORT MEASUREMENTS

U. Andriolo[1], F. Sancho[1], P. Freire[1] and F.S.B.F. Oliveira[1]

Abstract

Experiments on beach profile evolution and related sediment transport were carried out at LNEC's large wave flume. An eighteen-minute long record of an erosive wave condition impacting on sandy beach profile was video-monitored through a camera device looking at the wave flume lateral window. This included conceiving a sand-tracing procedure, which required setting a procedure to obtain a sand tracer with similar size and hydraulics properties as the native sand, and developing a video-image analysis technique capable of detecting and measuring dyed-sand areas on the video-frames, as well as tracking and calculating centre of mass displacement throughout the selected frame sequence. Preliminary results of the velocities of the dyed-sand centre of mass position along one record are shown and discussed. This technique allows obtaining intra-wave information of the sediment transport at the location of the video-records, complementing the time-integrated information gathered from bed profiling.

1. Introduction

In spite of recent advances in numerical simulations and instrumental techniques, the field of sediment dynamics still requires an important research effort to improve the performance of sedimentary-bed hydraulic facilities. In fact, the same complexities which hinder measurements are at the core of modeling issues. Within the European project Hydralab-IV, the joint research action WISE (Water Interface-Sediment Experiments) focused on the interaction of water and sediments. This aimed at improving the measurements of water velocity, sediment velocity/concentration, bed-forms and erosion/accretion rates at the interface of water and sediment, by means of both optical and acoustic devices. This work focuses on the former ones.

Optical systems in the laboratory are generally minimally intrusive and able to measure water/sediment velocities and concentrations at the water-sediment interface and in the water column. They usually provide instantaneous point measurements, although often one is interested in spatially-integrated measurements, such as bed-load fluxes.

Video-image data acquisition and processing is also, nowadays, a powerful and useful field monitoring technique, providing both qualitative and quantitative data on beach hydrodynamics and morphodynamics (e.g., Alexander and Holman, 2004; Holman and Stanley, 2007). Similarly, sediment tracers (coloured fluorescent sands) have been used in the field with great success in estimating (mostly alongshore) sediment fluxes and the thickness of the movable sediment layer (e.g., Ciavola *et al.*, 1997, Ferreira *et al.*, 2000).

In this paper, it is a new, low-cost, optical method for estimating the (intra-wave) cross-shore sediment transport, mainly at experimental facilities. This technique involves sediment dying, dimensioning and

[1] LNEC – National Laboratory for Civil Engineering, Av. do Brasil, 101, 1700-066 Lisbon, Portugal.
uandriolo@lnec.pt, fsancho@lnec.pt, pfreire@lnec.pt, foliveira@lnec.pt

placing of the coloured sediment tracers in the bed flume, video-monitoring of the tracers' displacement during the experiments, image processing, and estimating the tracers centre of mass displacements and relative velocities, at a given location along the beach cross-shore.

The experiments were also devised to evaluate the beach profile evolution under erosive and accretive wave conditions, as planned by the consortium of teams performing the same experiences in different facilities scales within the WISE joint research action.

2. Laboratory experiments

A new set of laboratory experiments have been performed at LNEC's large-scale irregular wave flume (COI2), with dimensions 73x3x2 m, aiming the evaluation of an innovative sediment transport measuring technique, described in section 3.

The test conditions were devised in conjunction with the experiments performed at the GWK and CIEM-UPC larger wave flumes. In particular, the GWK experiments were considered as the reference, i.e., as the prototype, and the experiments at COI2 were down-scaled in relation to those with a vertical length scale (n_h) of 1:4 (lab:prototype).

Moreover, following the scaling-laws' criterion proposed by van Rijn *et al*. (2011), a horizontal-to-vertical distorted model was adopted, where the horizontal length scale (n_L) is 1:5.6, and hence the distortion (n_h / n_L) is 1.41. This distortion resulted from a compromise between the flume dimensions, the input wave conditions (scaled according to the Froude number), and the available sand-bed characteristics (essentially, the type of material and the characteristic sediment dimensions). The bed material consisted in natural siliceous sand with an average d_{50} of 0.32 mm and geometrical spreading, defined as $(d_{84}/d_{16})^{0.5}$, of 1.57 (see the grain size distribution in Figure 1). Table 1 presents a few characteristics of the three flumes and of the bed sediment used in the respective experiments. Table 2 presents the input wave conditions for both, the erosive and the accretive, cases, tested in COI2 experiments.

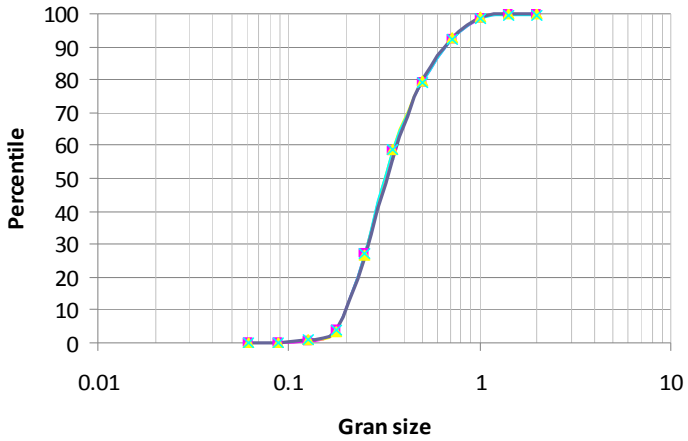

Figure 1. Grain size distribution of 4 samples of the bed material used in COI2 experiments.

Table 1. GWK, CIEM and COI2 flume characteristics.

Flume	Length (m)	Width (m)	Water depth (m)	Paddle	Horizontal scale	Vertical scale	d_{50} (mm)	Ws (cm/s)
GWK	300	5	5.00	Piston	Prototype	Prototype	0.35	4.9
CIEM	100	3	2.50	Wedge	1.9	1.9	0.25	3.4
COI2	73	3	1.19	Piston	5.6	4.0	0.32	3.8*

*Estimated according to Jiménez and Madsen (2003) formula, for $(\rho_s - \rho)/\rho = 1.58$

Table 2. Input wave conditions at COI2 experiments.

Wave conditions	H_s (cm)	T_p (s)	T_z (s)
Erosive	18.3	1.84	1.79
Accretive	16.0	2.26	2.13

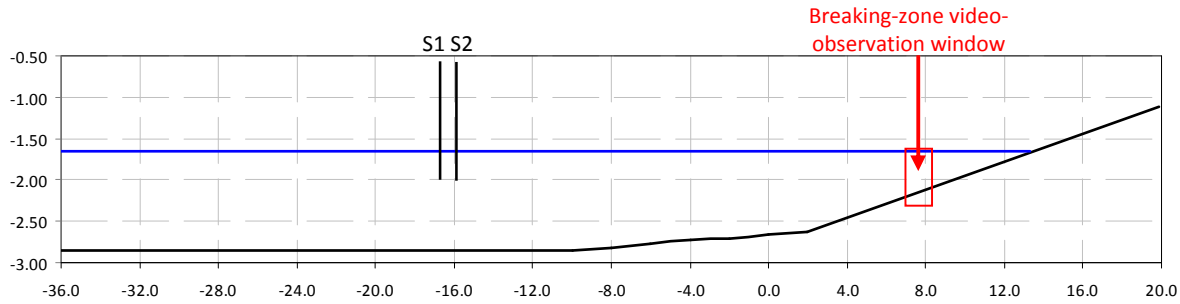

Figure 2. COI2 initial bed-profile (vertical and horizontal distances in meters, and distorted).

The experiments at LNEC started from an initial profile with a 1/10.6 slope in the active beach zone, corresponding to a 1/15 slope in the profiles tested in the GWK and CIEM flumes. This bed profile, formed by sand, matches the fixed, bottom of the flume at x=2 m (see Figure 2).

In the first phase of the experiments, which started from the planar beach profile, the erosive wave conditions series was input 11 times sequentially. Following the erosive wave conditions, in the second phase of the experiments, a sequence of 30 series of the accretive wave condition was imposed, nearly until a new equilibrium beach profile was reached. Each of the erosive and accretive wave time series lasted for 18 minutes and was interrupted during intervals of 5 minutes.

The values of the relevant parameters of the input wave conditions, which were the wave height and period (see Table 2), were measured at the starting of the profile, in the non-active zone located at the flat-bed region, for both the erosive and accretive experiments. The purpose of these measurements was the calibration and verification of the hydrodynamic input conditions.

Instrumentation along the flume was intentionally left to a minimum. Two wave gages (S1 and S2) were placed permanently at the end of the fixed flat-bed region, and one other (S3) was placed at the

middle of the video-measuring window in the surf zone. Figure 3 shows the free-surface elevation spectra from the records obtained during one of the accretive wave runs (the 8th time series), at the flat-bed and in the surf zone. Clearly, one observes the growth of lower frequency components from the starting of the surf zone to the swash region.

A pressure sensor was also installed: initially it was placed near the bottom in the swash region, and later it was moved to several other positions along the surf zone, during the input wave time series intervals. Finally, an electromagnetic current meter was installed in the same cross-shore position as the wave gage S3 (in the surf zone). Vertically, it was positioned nearly at half the water depth, at about 0.15 m below the still water level.

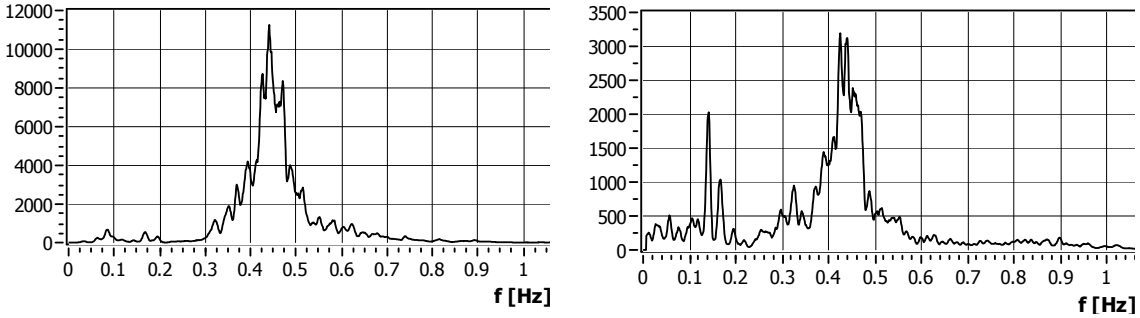

Figure 3. Wave spectra for the Accretive_08 test at: a) the flat-bed region (position S1); b) the surf zone region (S3).

The bed-profiles were measured at the end of a few, pre-defined wave runs (lasting 18 minutes each), according to the original plan, common also for the GWK and CIEM wave flumes. During all tests, bed ripples were formed everywhere, except for the erosive conditions in the surf zone. The bed level measuring technique (a vertical rod displaced every 10 cm along the horizontal plan) helped to filter out these bed ripples.

Figure 4 shows the bed profile evolution along the erosive and accretive wave conditions. Each number following the E or A prefixes corresponds to the wave run which is the order number of the input wave series of each phase experiment. The wave generator was positioned at the left (x=−36 m), out of the Figure 4, and the wave gages S2 and S1 were placed at x=−16, −17 m, respectively (see location in Figure 2).

In the erosive wave sequence, one observes an initial bar growth at x≈7.5 m, which crest was then displaced towards higher depth, at x≈6.5 m, and erosion at the beach foreshore. Basically, it appears that all eroded material was moved to the bar. Under the accretive waves sequence (which lasted three times longer than the erosive conditions) one sees the bar migration shoreward, but also the formation of a platform for x between 9-10 m. A minimal accretion is found at the water line.

3. Sand transport measurement technique

A new optic measurement technique for sediment transport in wave flume is presented, based on digital image processing of sediment bed motions video records obtained through the flume's lateral glass windows.

Prior to the physical experiment, a procedure to dye the sand grains with coated pigment was carried out, in order to obtain new coloured sand with the same or approximate grain size distribution and thus

the same hydraulics characteristics of the natural one (Foster and Lees, 2000). This included testing different components' proportions (cure, resin, diluent and sand) to have an acceptable and good detectable chroma in the video images. In particular, red and blue pigments were selected because they provided the best colour contrast in relation to the natural sand grains.

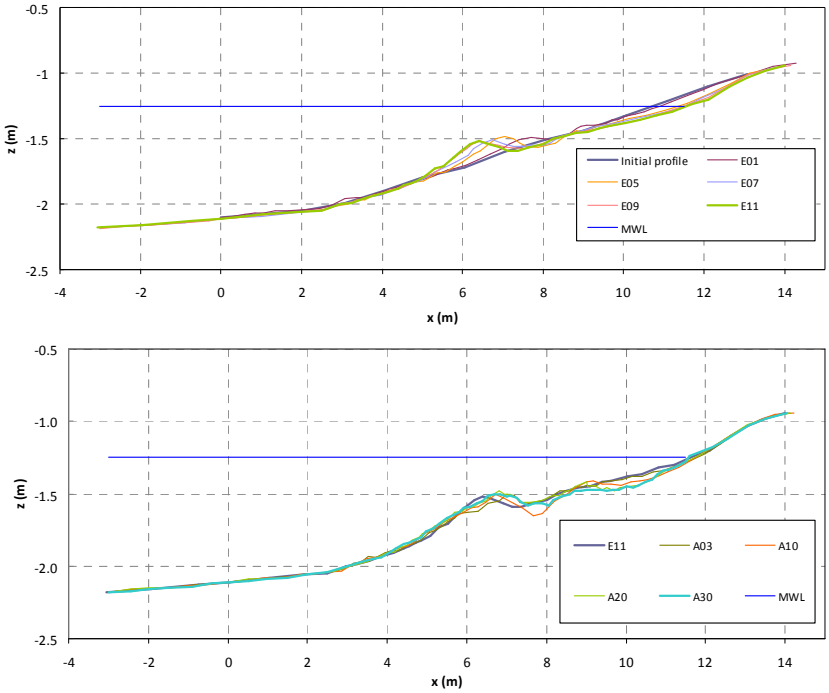

Figure 4. Profile evolution for the erosive (above) and accretive (below) wave conditions.

The adopted paint/sand volumetric ratio was 1/18. The paint was composed by 45% of pigment (from the sum of equal parts of cure and resin) and 55% of diluent, portioned by weight. Paint and sand were blended in a cement mixer (as performed in Silva *et al.*, 2007) for about one hour. Later, the dyed-sand was let to dry naturally over a plastic canvas for around 2 days. In a few cases, this dyed-sand was placed again in the mixer to help disaggregate some of the individual coloured grains that bonded together.

White and Inman (1989) reported that is tolerable a modal diameter mismatch between tracer sand and native sand on the order of 10%. Using the proportions indicated above, modal diameters determined from grain size distribution analysis show similar values, both for native and painted sands (red and blue): d_{50} diverged only around 1%. In terms of hydraulic properties, Black *et al.* (2007) recommends that the coated-particles density (specific gravity) not exceeds ±6% the native sediment's density. Here, red-painted grains average density resulted being within 1% higher than the original ones, whereas the blue-coated grains mean density was 6% lower (even if the red and blue pigments were mixed with the same cure, the outcome was two resin colours having a different behaviour). Hence, the laboratory analysis revealed that the coated sand is satisfying the recommendations in term of particle size and hydraulic properties found in the literature, so the quality of the experiments would not be affected.

The video-monitoring experimental set-up consisted in placing a Panasonic High Definition Camera (model HDC-SD9P/PC) looking sideways, about 1.3 m apart from the wave-flume lateral window, monitoring the sediment motion under the breaking zone. The camera was manually focused to acquire images of the sediment-water interface at 25 Hz frequency. Red- and blue-coated sand rectangular-sections of 6x6 cm^2, and 30 cm long (parallel to the flume's wave paddle direction, i.e., normal to the flume's lateral glass windows), were put in the desired places at the surface of the beach profile, amongst the natural coloured sand (see Figure 5, top panels).

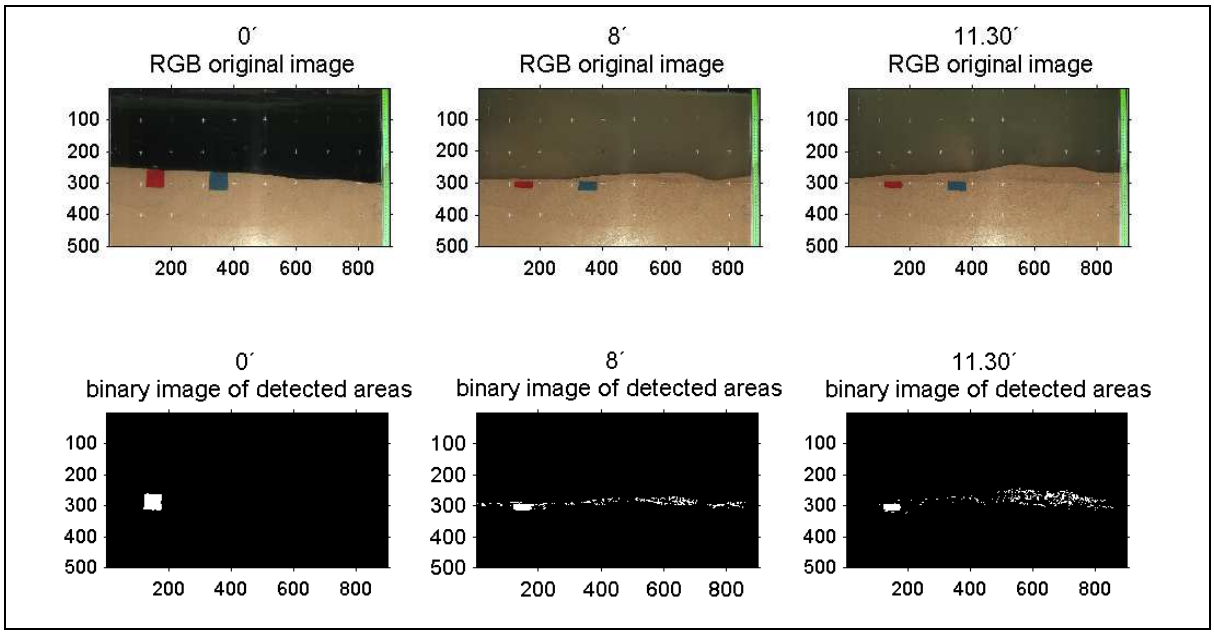

Figure 5. Example of original images obtained after frame-grabbing (above) and post-processed binary images (below) at the start of the experiment (minute 0), and after 8 and 11.30 minutes, respectively. Red coloured grains detected areas are given as white pixels in the binary images. Seaward movement is directed to the right of the picture.

For each erosive wave series, a video was stored and processed by frame-grabber software obtaining the related image sequence. For the present analysis, frames were selected every 1 minute, sequentially, and were corrected from distortion and rectified (Heikkilä and Silven, 1997), resulting in images of 900x500 pixels (the same size of the monitored area, 1 pixel corresponds to 1mm real). The imaging X-Y cartesian coordinate system origin was considered to be the left-top corner of image.

The images were processed by a semi-automatic Matlab code, aiming at detecting the location of the coated grains displaced by the wave induced currents. Colour theory is based on colour models that mathematically describe how colours may be represented: a colour space is one where the components of the colour model are precisely defined, typically, as three components (e.g., red, green and blue) or values (e.g., hue, saturation and brightness). Among several colour model representations tested for colour detection (such as RGB, HSV and colour spaces created by CIE Commission Internationale de l'Eclairage), CIELab colour space was found being the most suitable for the present aim (e.g., Melgosa, 2000). In this three-dimensional colour space model, the L stands for the lightness of the colour, with 0 representing black and 100 a diffuse white, the "a" is the redness versus greenness, while the "b" is the yellowness versus blueness.

The colour detection in CIELab is based on chromatic value calculated by the colour difference ΔE (Delta E), a number that shows the Euclidian distance between two colours. CIE proposed different formulas for the implementation of ΔE through the years: in this study, the colour difference is calculated using the equation CIE94 (CIE, 1995). Thus, a tolerance level for ΔE defines a region in the colour space, distinguishing what is acceptable (the colour is inside the tolerance space) and what is masked (pixels with colour components that are outside the tolerance region). The script was run twice, setting two different tolerance values in order to discriminate the level of dyed-sand grains' densities (one for the initial red area, and a second one for predominant red-sand amongst the natural sand grains). The detected areas were transformed as white pixels in two binary images that were merged together, representing all the pixels where red-sand predominant (see Figure 5, lower panels).

4. Sediment-tracer velocities: method and results

The Spatial Integration Method (abbreviated here by SIM) commonly allows to evaluate the alongshore sediment transport in a 3-dimensional way (e.g., Komar and Inman, 1970). This study is an attempt to apply the SIM to evaluate cross-shore sediment in two dimensions.

In the present method, each post-processed binary image, with the clear identification of the coloured-sand, was divided in a 20x20 mm^2 grid (image size is 900x500 mm^2). For each of the 20x20 mm^2 squares with identified white pixels, the center of mass of those pixels was calculated.

Then, the total centre of mass position in each image frame was calculated by associative addition:

$$X_c = \frac{\sum_1^n A_n x_n}{A_{tot}}, \qquad Y_c = \frac{\sum_1^n A_n y_n}{A_{tot}}$$

where (X_c, Y_c) are the coordinates of the tracer centre of mass, n is the number of detected coloured portions, A_n the related area, and (x_n, y_n) the centroid coordinates.

The horizontal and vertical velocities, (V_x, V_y), of the sediment's centre of mass are computed as (Madsen, 1987):

$$V_x = \frac{X_{c,t2} - X_{c,t1}}{t_2 - t_1}, \qquad V_y = \frac{Y_{c,t2} - Y_{c,t1}}{t_2 - t_1}$$

where t_2 and t_1 are two instants in the image sequence.

This velocity does not correspond to the velocity of the bed-load motion (which, in the breaking zone, occurs often in the sheet-flow regime), because what is being calculated is the motion of the sand grains, no matter if they were carried as bed-load or in suspension mode. Hence, this corresponds to an average velocity of the displaced sand grains, and thus should be related to the total sediment transport. The sediment transport rate can then be determined by the product of sediment's centre of mass velocity by the mixing layer thickness. The mixing layer can be computed by the thickness of coloured sand that was removed in the considered interval. In the following, only the sediment's centre of mass velocities will be presented and discussed.

The preliminary results of the application of the above methodology are given below, only for the red coloured areas. Thus, from the selected and processed frames of the video images acquired during the wave runs, the areas of red-painted sand grains (see Figure 5) and their centroids within each squared-grid are obtained, and the centre of mass position of the total red-coloured area is calculated along the experiment. Furthermore, the centres of mass average velocities are calculated (see Table 3).

It is worth noticing that the total area was generally increasing with the duration of the wave run, which indicates a spread of the initially concentrated red-sands. This does not correspond to a (unrealistic) growth of the total red-sand mass, but is a feature of the processing algorithm as it does

not count red-grains (which are approximately three times smaller than the pixel resolution of 1mm), but detects the pixels where red-sand predominates. Since the red-sand detection algorithm also depends on the colour-model and ΔE threshold (which is adjusted according to the ambient light and other colour and light properties), it is natural that the total red-sand area varies from one image to another.

Table 3: Total red-coloured area, centre of mass position, and velocities, V_x, V_y, at given instants within the experiment.

Minute	Frame number	Total Red Area (mm^2)	Centre of mass position X, Y (mm)	*Vx* (mm/sec)	*Vy* (mm/sec)
0	0000	3101	147.4, 287.6		
2	3000	2514	227.0, 294.8	0.663	0.060
3	4500	4419	391.6, 288.0	2.743	-0.113
4	6000	2305	302.0, 297.1	-1.493	0.151
5	7500	2189	262.5, 300.4	-0.659	0.056
6	9000	2608	274.4, 297.1	0.198	-0.055
7	10500	4937	313.9, 292.8	0.659	-0.072
8	13000	4133	419.7, 294.4	1.058	0.015
11’30	17250	4550	510.3, 284.5	0.533	-0.058
18	27000	7083	492.9, 282.8	-0.045	-0.004

Figure 6 shows the centre of mass displacements through the whole experiment. At the end of the first erosive wave series (lasting 18 minutes, H_s=0.183 m and T_p=1.84 s), the centre of mass was found 345 mm seaward from the initial position (345.5 mm in the x direction, -4.8 mm in the y direction). Analyzing its path, it was registered 362.9 mm maximum displacement in x direction at 11’30 minute, whereas maximum vertical relocations were 12.8 mm at frame 7500 (remembering that y increases from top to bottom in the vertical plan) and -4.8 mm at minute 18, among the selected frames. From this figure, one clearly sees that not only the path of the moving sand mass center is not constant in time, but that it has also several phases. In the first phase, from the starting to minute 3, it moved rapidly seaward; then, from minute 3 to 5, it moved shoreward, although from minute 4 to 7 one can say that the centre of mass remained within a 5 cm region, i.e., the net transport was nearly null; the third phase corresponds to that observed from minute 7 to 11.5, with a significant net seaward movement, but not as intense as in the first 3 minutes.

The time variation of the centre of mass horizontal and vertical velocities is shown in Figure 7. Here, one observes that the majority of the computed horizontal velocities are smaller than 1mm/s, and also than only two observations are negative (shoreward) velocities. Thus, it dominated the net seaward sand transport under the erosive wave conditions, as observed from the breaker-bar growth (see Figure

4). The largest horizontal velocities are attained at the start of the experiment, where the bed tends to adjust faster to the incoming wave conditions.

In terms of vertical motions, one expected the vertical velocity to be around zero, as near bed motions due to the waves induced currents are predominantly horizontal in shallow waters and mild sloping beaches. Hence it is expected that the vertical velocity scales with the horizontal velocity with a ratio equal to the bed slope. Indeed, one observes that the vertical velocities are approximately 10 times smaller than the horizontal velocities.

These tendencies and results shall be compared with the sediment transport rates computed from the measured beach profiles, using the sediment mass conservation equation (often designated by the Exner equation). However, the present analysis allows getting an intra-wave picture of the sediment motions.

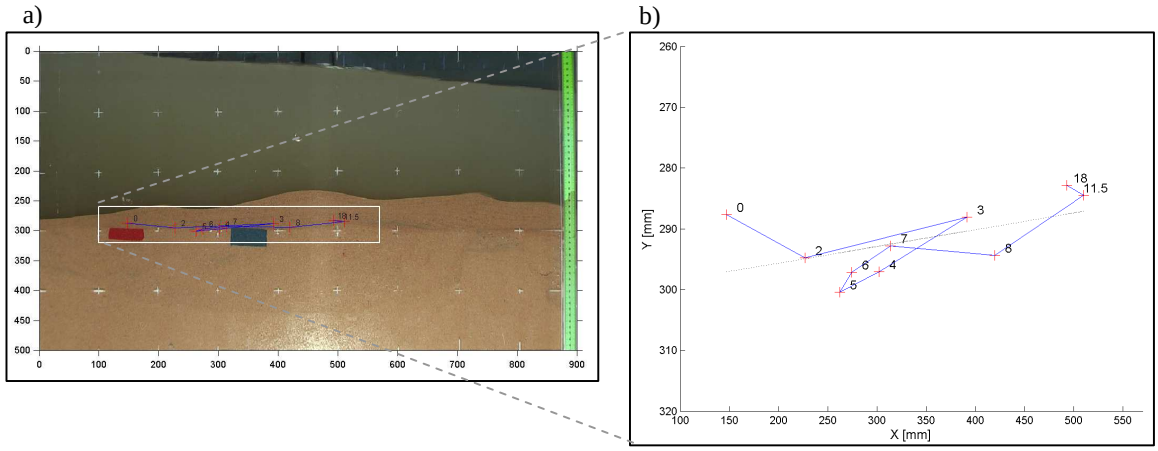

Figure 6. a) Rgb image frame at minute 18, centre of mass positions and path; the white rectangle shows the area represented at the right; b) Distorted x-y image, with the positions of the red tracers centre of mass (red crosses) through the 18 minutes wave series; the numbers associated to the crosses indicate the time in minute. Blue line connects the points in sorted order. Dotted black line is the linear regression line.

5. Conclusions

This paper presents a new, low-cost, optical method for estimating the (intra-wave) cross-shore sediment transport, mainly at experimental facilities. This methodology evolved from combining existing (field-site) video monitoring systems with sediment tracer techniques.

A new set of experiments were also carried out at COI2 (LNEC's) wave flume to evaluate the beach profile evolution under erosive and accretive wave conditions, using distorted vertical/horizontal length scales when comparing with similar experiments performed at larger scales at the GWK and CIEM wave flumes.

An eighteen-minute long record of an erosive wave condition impacting on sandy beach profile was video-monitored through a camera device looking at the wave flume lateral window. The developed video-image processing procedure was capable of detecting and measuring dyed-sand areas in the frames, as well as tracking and calculating the centre of mass displacements through the selected frame sequence.

The preliminary analysis shows an interesting correlation between velocity and relocations of weighted mass center. Further analysis involving the blue sand-coloured detection and associating the

wave series is needed, in order to make a final conclusion regarding the potential suitability of the optical technique for evaluating and understanding of the cross-shore sediment transport rate.

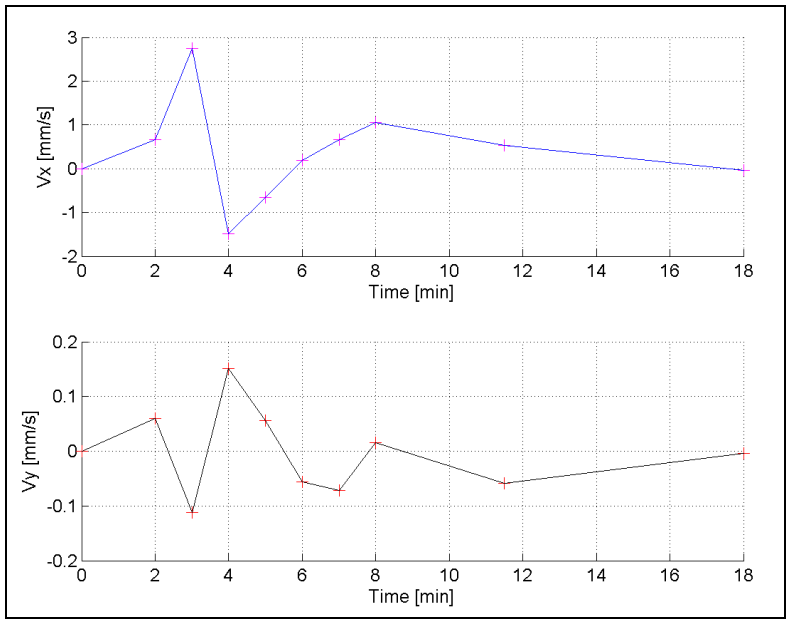

Figure 7. Mean horizontal (above) and vertical (below) velocities of the centre of mass motion.

Acknowledgements

This work was performed within the scope of the Joint Research Initiative WISE (Water Interface Sediment Experiment) of the "Hydralab IV – More than Water" project, contract number 261520, financed by the European Union 7th Framework Programme. The authors thank Mr. Simões Pedro and Vitor Pisco for their endless collaboration during the laboratory experiments.

References

Alexander, P.S., Holman, R.A. (2004). Quantitative analysis of nearshore morphological variability based on video imaging. *Marine Geology*, 208, 101–111.

Black ,K, Athey, S. Wilson, P., Evans, D., 2007. The use of particle tracking in sediment transport studies: a review. In Balson, P.S. & Collins, M.B., *Coastal and Shelf Sediment Transport*. Geological Society of London, 2007, Special Publication, 274pp.

Ciavola P., Taborda R., Ferreira O., Dias J.M.A. (1997). Field measurements of longshore sand transport and control processes on a steep meso-tidal beach in Portugal. *J. Coastal Res.*, 13:1119–1129.

CIE Publication 116-1995, Industrial colour-difference evaluation. Vienna. CIE Central Bureau.

Ferreira O., Ciavola P., Taborda R., Bairros M., Dias J.M.A. (2000). Sediment mixing depth determination for steep and gentle foreshores *J. Coastal Res*., 16:830–839.

Foster, I.D.L. and Lees, J.A., 2000. Tracers in geomorphology: theory and applications in tracing fine particulate sediments. In *Tracers In Geomorphology*, edited by Foster I.D.L.,2000, John Wiley & Sons Ltd, Chichester,560 pp.

Heikkilä, J, Silvén, A., 1997. Four-step Camera Calibration Procedure with Implicit Image Correction. Computer Vision and Pattern Recognition, 1997. Proceedings, IEEE Computer Society Conference.

Holman, R.A., J. Stanley (2007). The history and technical capabilities of Argus. Coastal Engineering, 54, 477–491.

Jiménez, J.A. and O.S. Madsen, 2003. A Simple Formula to Estimate Settling Velocity of Natural Sediments. *Journal of Waterway, Port, Coastal, and Ocean Engineering*, Vol. 129, No. 2, 70.-78.

Komar, P.D. and D.L. Inman, 1970. Longshore sand transport on beaches. *Journal of Geophysical Research*, Oceans and Atmospheres, Volume 75, Issue 30, 5914–5927.

Madsen, O.S., 1987. Use of tracers in sediment transport studies. *Proceeding Coastal Sediments*. ASCE, New York, pp. 424 – 435.

Melgosa, M., 2000. Testing CIELAB-based color-difference formulas. *Color Research and Application*, Vol. 25. Issue 1, pp 49–55.

Silva, A., Taborda, R., Rodrigues, A., Duarte, J., Cascalho, J., 2007. Longshore drift estimation using fluorescent tracers: New insights from an experiment at Comporta Beach, Portugal. *Marine Geology*, Vol. 240, Issue 1-4, pp. 137-150.

Van Rijn, L.C., Tonnon, P.K., Sánchez-Arcilla, A., Cáceres, I., Grüne, J., 2011. Scaling laws for beach and dune erosion processes. *Coastal Engineering*, 58, pp. 623–636, doi:10.1016/j.coastaleng.2011.01.008.

White, T., Inman, D., 1989. Application of tracer theory to NSTS experiments. In: *Nearshore Sediment Transport*, edited by Seymor R.J., Plenum NY, 115–128

http://www.vision.caltech.edu/bouguetj/calib_doc/index.html Last access May 2013.